VNU Journal of Science: Mathematics - Physics

Journal homepage: https://js.vnu.edu.vn/MaP

Original Article

Effects of Hole Transport Layer Thickness on Photovoltaic Performance of Perovskite Solar Cell

Dao Quang Duy*

VNU Vietnam Japan University, Luu Huu Phuoc, Thanh Xuan, Hanoi, Vietnam

Received 4th August 2025
Revised 25th September 2025; Accepted 02nd March 2026

Abstract: We demonstrate effects of thickness of liquid-crystalline based hole transport layer (HTL) on photovoltaic performance of perovskite solar cell (PSC). A 70 nm thick HTL resulted in a device achieving a power conversion efficiency (PCE) of 9.8% under reverse bias scanning. Increasing the liquid-crystalline based HTL thickness to 100 nm improved device performance, yielding a PCE of 11.4%, indicating enhanced interfacial contact and more effective coverage of HTL over the $CH_3NH_3PbI_3$ perovskite absorber. Notably, the hysteresis index decreased with increasing the liquid-crystalline based HTL thickness, suggesting mitigation of charge accumulation at the interfacial layers and reduction of the hysteresis phenomena in PSCs.

Keywords: Perovskite solar cell, thin film, wet processing, hole transport layer.

1. Introduction

Because of growing global concern over environmental sustainability, renewable energy technologies such as wind, hydroelectric, and solar have garnered substantial interest. Among these, perovskite solar cells (PSCs) have emerged as a highly promising next-generation photovoltaic technology, owing to their unique attributes including broad absorption spectra, low-cost and solution-processable precursors, and long exciton diffusion lengths [1-4]. The first PSC achieving a power conversion efficiency (PCE) above 3% was reported by Myasaka in 2009; however, a major milestone was reached in 2012 when Snaith introduced a solid-state PSC with a PCE exceeding 10% [5, 6]. Since then, both the efficiency and operational stability of PSCs have advanced significantly, driven by innovations in thin-film deposition techniques, device architecture optimization, charge transport layer engineering, and interfacial modification strategies [7-10].

* Corresponding author.
E-mail address: dq.duy@vju.ac.vn

https//doi.org/10.25073/2588-1124/vnumap.5056

To facilitate efficient transport of photogenerated charge carriers, PSCs commonly employ an electron transport layer (ETL) and a hole transport layer (HTL) [8, 11]. ETLs, typically composed of robust inorganic materials, often feature a bilayer architecture consisting of a compact thin film and a mesoporous scaffold. The compact ETL serves as an electron-selective contact and a barrier to hole transport, while the mesoporous layer promotes perovskite infiltration and crystallization. Surface engineering of the ETL, particularly by minimizing surface hydroxyl groups and physisorbed water, is critical to suppressing undesirable PbI_2 crystallization, thereby improving perovskite film quality [8]. On the other hand, HTLs must satisfy several essential criteria for effective hole extraction: i) The highest occupied molecular orbital (HOMO) level should be well-aligned with the valence band of the perovskite to facilitate efficient hole transfer; ii) The lowest unoccupied molecular orbital (LUMO) level must be sufficiently high to prevent electron back-transfer; iii) The material should exhibit high hole mobility to reduce resistive losses; and iv) Thermal and photochemical stability, along with hydrophobicity, are necessary to enhance device longevity by protecting the perovskite absorber from moisture and environmental degradation [12].

Recently, liquid crystalline materials have garnered significant attention as promising small-molecule semiconductors for thin-film optoelectronic fields because of their excellent properties, such as high charge carrier mobility and good solubility in organic solvents [13]. Organic solar cells incorporating the liquid crystalline donor achieved PCEs exceeding 5.2%, while PSCs employing a liquid-crystalline based HTL demonstrated PCEs above 16% [14, 15]. In the present study, we report the fabrication of high-efficiency PSCs employing non-peripherally substituted octapentyl phthalocyanine (C_5PcH_2) as the HTL and the influence of HTL thickness on the photovoltaic performance of the devices.

2. Experimental Procedure

The PSC in n-i-p structure was synthesized following the previously reported procedures on patterned fluorine doped tin oxide (FTO) substrates with an active area of approximately 0.24 cm^2 [16, 17]. The compact TiO_2 ETL (ca. 50 nm) was deposited via a spraying method (300 µL of titanium diisopropoxide bis(acetylacetonate) in 4 mL ethanol), while mesoporous TiO_2 film (ca. 300 nm) was spin-coated using TiO_2 nanoparticles (DSL 18NR-T; DYESOL). Both TiO_2 layers were treated in an aqueous solution of $TiCl_4$ (Wako) (220 µL $TiCl_4$ mixed with 100 mL water) at 70 ºC for 20 minutes. The $CH_3NH_3PbI_3$ perovskite absorber (ca. 400 nm) was spin-coated inside an N_2-filled glovebox using a mixed precursor solution containing CH_3NH_3I (1.1 M; Tokyo Chemical Industry Co.) and PbI_2 (1.1 M; Tokyo Chemical Industry Co.) in dimethylsulphoxide (DMSO). The HTLs were synthesized by spin-coating a solution of C_5PcH_2 in chloroform solvent. The thickness of the C_5PcH_2 HTL was modulated by varying the solution concentration from 7 mg/mL to 16 mg/mL. Post-deposition, the films were thermally annealed at 130 °C for 10 minutes to enhance crystallinity and remove residual organic solvents. Finally, gold (Au) electrodes with a thickness of 80 nm were thermally evaporated through a shadow mask under a vacuum of approximately 3×10^{-5} Torr to complete the device architecture.

The current density–voltage (*J–V*) characteristics of the fabricated PSCs were measured using a 6243 DC voltage-current source/monitor under simulated AM 1.5G solar irradiation, provided by a WXS-50S-1.5 solar simulator. The illumination intensity was calibrated to 100 mW/cm^2 using a certified monocrystalline silicon reference cell. The *J-V* characteristics were estimated under both reverse (from forward bias to short circuit) and forward (from short circuit to forward bias) scans. The scan rates and signal integration time are adjusted to achieve the minimum hysteresis index (*HI*). In particular, the step sizes and signal integration time are 0.0065 V and 0.0167 s for reverse bias scans and are 0.026 V and 1.67 s for forward bias scans. Both of them are performed in a range from -0.1 V

to 1.2 V. Optical absorption spectra were obtained using a UV–Vis–NIR spectrophotometer (Shimadzu UV-3150), while photoluminescence (PL) spectra were recorded with a fluorescence spectrophotometer (Hitachi F-4500) using an excitation wavelength of 500 nm for all PL measurements. Film thicknesses were determined with a surface profilometer (Dektak 150). The ionization potential of the C_5PcH_2 thin films was measured using photoelectron yield spectroscopy (Sumitomo Heavy Industries PYS-202-H). Measurements were performed under a low vacuum of approximately 3×10^{-1} Pa.

3. Results and Discussion

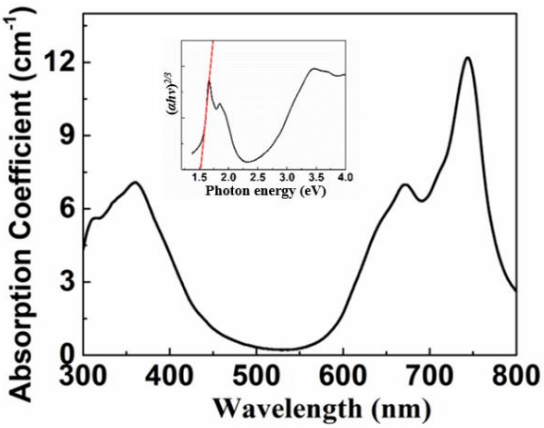

Figure 1. Optical absorption coefficient spectrum of C_5PcH_2 molecules. The inset Figure is Tauc plot $((\alpha hv)^{2/3}$ versus photon energy).

Figure 1 presents the optical absorption coefficient spectra of C_5PcH_2 in solid-state thin-film form. The spectra exhibit two prominent absorption bands centered at approximately 735 nm and 360 nm, corresponding to the Q-band and B-band (Soret-band) transitions, respectively, features that are characteristic of tetrapyrrolic porphyrinoid complexes [18, 19]. The absorption onset was 809 nm. The optical band gap of the C_5PcH_2 molecules was then determined from the absorption data using Tauc's relation [20], which expressed in Equation (1):

$$\alpha hv = C(hv - E_g)^{\beta} \quad (1)$$

Where C is a proportionality constant known as the band tailing parameter, and hv represents photon energy. The symbol α denotes the absorption coefficient, while β is an exponent that depends on the nature of the electronic transitions. Since the Q-band absorption of the C_5PcH_2 molecule originates from the direct forbidden transitions [19, 21], we fitted Tauc's plot using a β value of 3/2, as shown in the inset of Figure 1. Based on this analysis, the optical band gap of the C_5PcH_2 molecules was estimated to be 1.52 eV.

The ionization potential spectrum of the C_5PcH_2 molecule was also measured, as shown in Figure 2. The C_5PcH_2 molecule exhibits a HOMO energy level of 5.17 eV, from which the LUMO energy level is estimated to be approximately 3.7 eV. For reference, the HOMO and LUMO energy levels of the $CH_3NH_3PbI_3$ perovskite materials are well-documented to be approximately 5.4 eV and 3.9 eV, respectively [22]. The relatively deep HOMO level of C_5PcH_2 promotes efficient hole extraction from the perovskite layer, while its shallower LUMO level acts as an electron-blocking barrier, effectively

suppressing charge recombination at the interface. This favorable energy level alignment highlights the potential of C_5PcH_2 as a viable hole transport material for high-performance PSCs.

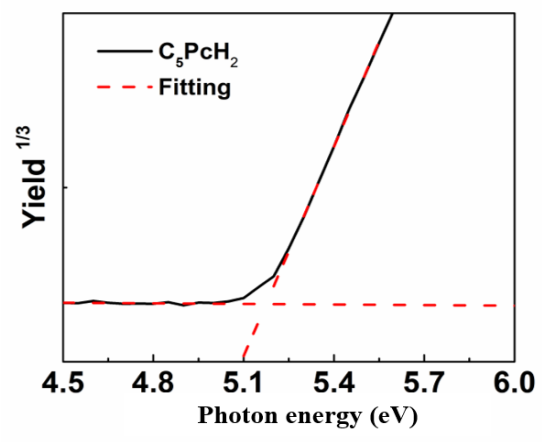

Figure 2. Ionization potential spectrum of C_5PcH_2 molecules.

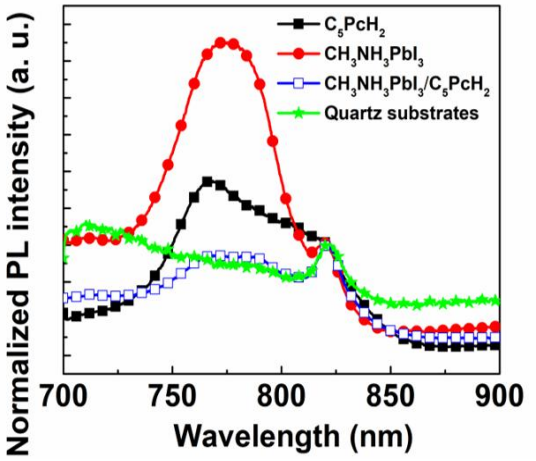

Figure 3. PL spectra of materials in this study.

PL spectra of the $CH_3NH_3PbI_3$ perovskite and the C_5PcH_2 HTL were measured out, as shown in Figure 3. Herein, the thin film thicknesses are approximately 100 nm and 400 nm for the C_5PcH_2 HTL and $CH_3NH_3PbI_3$ perovskite, respectively. The $CH_3NH_3PbI_3$ perovskite absorber displays a broad PL emission peak centered around 775 nm, while C_5PcH_2 HTL shows a distinct emission peak at approximately 767 nm. A weak emission feature observed near 825 nm is attributed to the parasitic light originating the fluorescence spectrophotometer. To evaluate the interfacial compatibility of the C_5PcH_2 HTL with the perovskite layer, the PL quenching of the perovskite/C_5PcH_2 heterojunction was analyzed. Notably, a significant reduction in PL intensity was observed upon deposition of the C_5PcH_2 layer atop of the $CH_3NH_3PbI_3$ perovskite films. This pronounced quenching effect indicates efficient hole extraction and transport from the $CH_3NH_3PbI_3$ perovskite layer to the C_5PcH_2 HTL, confirming its suitability for facilitating charge transfer toward the Au anode in PSCs.

Figure 4 shows the *J-V* characteristics of PSCs employing the C_5PcH_2 molecule as an HTL. During forward bias scanning, the devices with a 70 nm thick C_5PcH_2-HTL exhibit a short-circuit current density (J_{SC}) of 15.6 mA/cm^2 and the open-circuit voltage (V_{OC}) of 0.91 V. With the fill factor (*FF*) of 0.49, these devices reach a PCE of 7%. Notably, under reverse bias scanning, the PCE improves to 9.8%, accompanied by a *HI* of 0.28, as shown in Table 1. We note that HI is calculated as Equation (2):

$$HI = \frac{PCE_{\mathrm{RS}} - PCE_{\mathrm{FS}}}{PCE_{RS}} \quad (2)$$

Herein, PCE_{RS} and PCE_{FS} are PCEs of the cells in reverse and forward bias scans, respectively. The observed performance enhancement is primarily attributed to increases in the *FF* (0.57) and J_{SC} (18.5 mA/cm^2), while V_{OC} (0.93 V) remained nearly constant. The strong dependence of photovoltaic characteristics on voltage sweep direction indicates pronounced *J-V* hysteresis in the fabricated devices. Although further investigation is required to fully unravel the underlying mechanisms responsible for this hysteretic behavior, we suggest that this hysteresis may result from charge transfer rates at interfaces within the perovskite absorber of the conventional n-i-p structure, and/or slow charge trapping and de-trapping phenomena within perovskite defects [23].

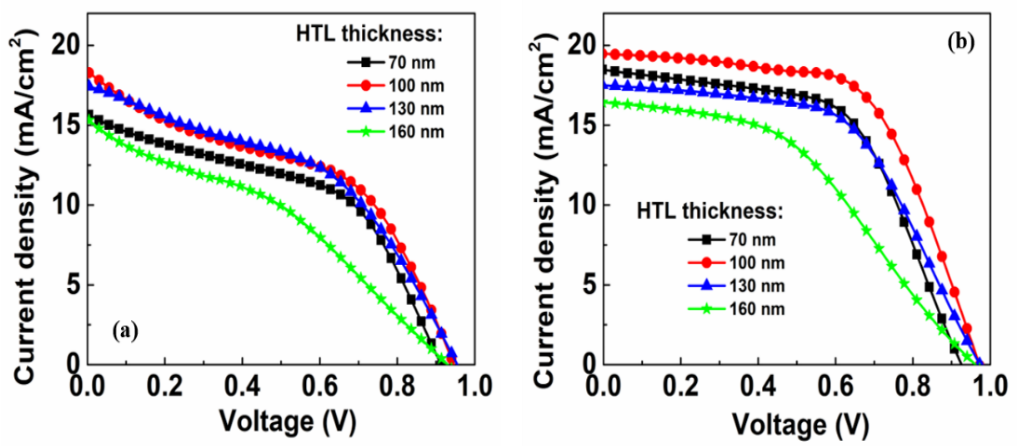

Figure 4. *J-V* curves of PSCs utilizing C_5PcH_2 HTL with different thickness under (a) forward bias scan and (b) reverse bias scan.

Table 1. Dependence of *HI* on C_5PcH_2 HTL thickness

C_5PcH_2 HTL thickness	70 nm	100 nm	130 nm	160 nm
HI	0.28	0.30	0.22	0.27

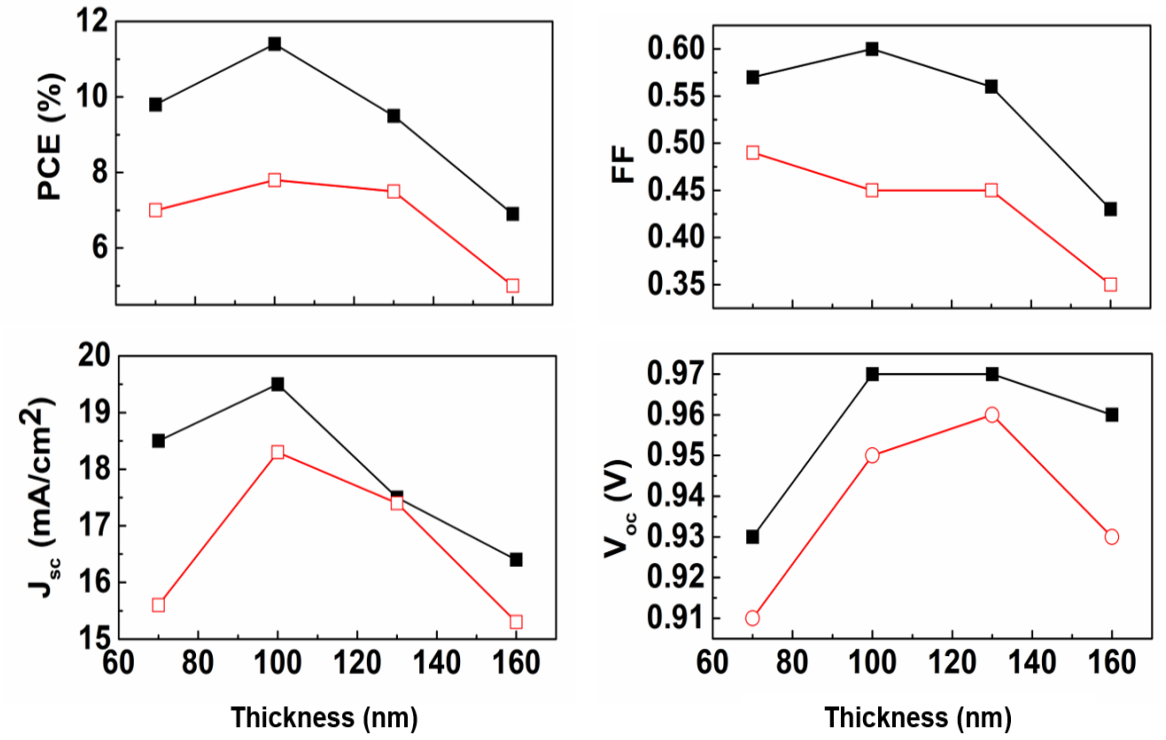

Figure 5. Dependence of photovoltaic properties of the fabricated PSCs on HTL thickness under reverse bias scan (filled rectangles) and forward bias scan (empty rectangles).

Furthermore, the influence of C_5PcH_2 HTL thickness on the photovoltaic performance of the PSCs was systematically investigated, as illustrated in Figure 5. As the HTL thickness increased from 70 nm to 100 nm, the PCE improved to 7.8% and 11.4% under forward and reverse bias scans, respectively. This enhancement is accompanied by concurrent improvements in all key photovoltaic parameters, J_{SC}, V_{OC}, and *FF*, suggesting improved interfacial contact and more uniform coverage of the C_5PcH_2 HTL over the $CH_3NH_3PbI_3$ perovskite absorber.

However, further increasing the HTL thickness to 160 nm led to a noticeable decline in device performance, with the PCE decreasing to 5.0% and 6.9% under forward and reverse scans, respectively. This degradation is attributed to elevated series resistance induced by the thicker HTL, which impedes charge transport and extraction, thereby lowering overall device efficiency. Notably, the HI was reduced to 0.22 and 0.27 as the HTL thickness increased to 130 nm and 160 nm, respectively. While further investigation is needed to fully elucidate the origin of *J–V* hysteresis, the observed trend suggests that increased HTL thickness partially mitigates charge accumulation at interfacial regions, contributing to the suppression of hysteresis phenomena in PSCs.

4. Conclusion

In summary, the high-efficient PSC employing C_5PcH_2 as a HTL was successfully fabricated, and the impact of HTL thickness on device performance was systematically investigated. At an HTL thickness of 70 nm, the device exhibited the PCEs of 7.0% and 9.8% under forward and reverse bias scans, respectively. Increasing the C_5PcH_2 HTL thickness to 100 nm resulted in enhanced PCEs of 7.8% (forward) and 11.4% (reverse), attributed to improved interfacial contact and more uniform coverage of the HTL over the $CH_3NH_3PbI_3$ perovskite absorber. Additionally, the *HI* decreased slightly with increasing HTL thickness, suggesting that a thicker HTL may partially suppress interfacial charge accumulation, thereby mitigating *J–V* hysteresis. These findings underscore the critical role of HTL thickness in optimizing both the efficiency and stability of PSCs.

Acknowledgments

This research is funded by Vietnam National Foundation for Science and Technology Development (NAFOSTED) under grant number 103.02-2024.07. The author also thanks Prof. Ryotaro Tsuji (Kaneka Corporation, Japan), Prof. Akihiko Fujii (Osaka University, Japan), and Prof. Masanori Ozaki (Osaka University, Japan) for their material and equipment support.

References

[1] M. A. Green, E. D. Dunlop, M. Yoshita, N. Kopidakis, K. Bothe, G. Siefer, X. Hao, Solar Cell Efficiency Tables (Version 63), Progress in Photovoltaics, Vol. 32, 2024, pp. 3-13, https://doi.org/10.1002/pip.3750.

[2] S. D. Stranks, G. E. Eperon, G. Grancini, C. Menelaou, M. J. P. Alcocer, T. Leijtens, L. M. Herz, A. Petrozza, H. J. Snaith, Electron-Hole Diffusion Lengths Exceeding 1 Micrometer in an Organometal Trihalide Perovskite Absorber, Science, Vol. 342, 2013, pp. 341-344, https://doi.org/10.1126/science.1243982.

[3] H. S. Jung, N. Park, Perovskite Solar Cells: From Materials to Devices, Small, Vol. 11, 2015, pp. 10-25, https://doi.org/10.1002/smll.201402767.

[4] J. Han, K. Park, S. Tan, Y. Vaynzof, J. Xue, E. W. G. Diau, M. G. Bawendi, J. W. Lee, I. Jeon, Perovskite Solar Cells, Nature Reviews Methods Primers, Vol. 5, 2025, pp. 3, https://doi.org/10.1038/s43586-024-00373-9.

[5] M. M. Lee, J. Teuscher, T. Miyasaka, T. N. Murakami, H. J. Snaith, Efficient Hybrid Solar Cells Based on Meso-Superstructured Organometal Halide Perovskites, Science, Vol. 338, 2012, pp. 643-647, https://doi.org/10.1126/science.1228604.
[6] A. Kojima, K. Teshima, Y. Shirai, T. Miyasaka, Organometal Halide Perovskites as Visible-Light Sensitizers for Photovoltaic Cells, J. Am. Chem. Soc., Vol. 131, 2009, pp. 6050-6051, https://doi.org/10.1021/ja809598r.
[7] N. S. Kumar and K. C. B. Naidu, A Review on Perovskite Solar Cells (Pscs), Materials and Applications, Journal of Materiomics, Vol. 7, No. 5, 2021, pp. 940-956, https://doi.org/10.1016/j.jmat.2021.04.002.
[8] D. Q. Duy, A. Fujii, R. Tsuji, N. H. Pham, B. H. Van, C. D. Sai, N. D. Thien, V. T. Huong, M. Ozaki, Mesoporous TiO2 Electron Transport Layer Engineering for Efficient Inorganic-organic Hybrid Perovskite Solar Cells Using Hydrochloric Acid Treatment, Thin Solid Films, Vol. 732, 2021, pp. 138768, https://doi.org/10.1016/j.tsf.2021.138768.
[9] S. Gan, H. Sun, C. Li, L. Li, Bifacial Perovskite Solar Cells: a Universal Component that Goes Beyond Albedo Utilization, Science Bulletin, Vol. 68, 2023, pp. 2247-2267, https://doi.org/10.1016/j.scib.2023.08.043.
[10] M. A. Green, E. D. Dunlop, M. Yoshita, N. Kopidakis, K. Bothe, G. Siefer, D. Hinken, M. Rauer, J. Hohl-Ebinger, X. Hao, Solar Cell Efficiency Tables (Version 64), Progress in Photovoltaics: Research and Applications, Vol. 32, 2024, pp. 425-441, https://doi.org/10.1002/pip.3831.
[11] D. Q. Duy, A. Fujii, R. Tsuji, Y. Takeoka, M. Ozaki, Efficiency Enhancement in Perovskite Solar Cell Utilizing Solution-Processable Phthalocyanine Hole Transport Layer with Thermal Annealing, Org. Electron., Vol. 43, 2017, pp. 156-161, https://doi.org/10.1016/j.orgel.2017.01.027.
[12] C. Zhang, K. Wei, J. Hu, X. Cai, G. Du, J. Deng, Z. Luo, X. Zhang, Y. Wang, L. Yang, J. Zhang, A Review on Organic Hole Transport Materials for Perovskite Solar Cells: Structure, Composition and Reliability, Materials Today, Vol. 67, 2023, pp. 518-547, https://doi.org/10.1016/j.mattod.2023.06.009.
[13] D. Q. Duy, K. Watanabe, H. Itani, L. Sosa-Vargas, A. Fujii, Y. Shimizu, M. Ozaki, Octahexyltetrabenzotriazaporphyrin: A Discotic Liquid Crystalline Donor for High-performance Small-molecule Solar Cells, Chem. Lett. Vol. 43, 2014, pp 1761-1763, https://doi.org/10.1246/cl.140685.
[14] D. Q. Duy, A. Fujii, R. Tsuji, M. Ozaki, Highly Efficient Perovskite Solar Cell Utilizing a Solution-processable Tetrabenzoporphyrin Hole Transport Material with p-type Dopants, Applied Physics Express, Vol. 12, 2019, pp. 112009, https://doi.org/10.7567/1882-0786/ab4aa2.
[15] D. Q. Duy, L. S. Vargas, T. Higashi, M. Ohmori, H. Itani, A. Fujii, Y. Shimizu, M. Ozaki, Efficiency Enhancement in Solution Processed Small-molecule Based Organic Solar Cells Utilizing Various Phthalocyanine–tetrabenzoporphyrin Hybrid Macrocycles, Org. Electron., Vol. 23, 2015, pp. 44-52, https://doi.org/10.1016/j.orgel.2015.04.009.
[16] D. Q. Duy, Fabrication of Highly Efficient Pervoskite Solar Cells Using Simple Single-step Solution Method, VNU Journal of Science: Mathematics – Physics, Vol. 37, No. 2, 2021, pp. 69-76, https://doi.org/10.25073/2588-1124/vnumap.4557.
[17] N. J. Jeon, J. H. Noh, Y. C. Kim, W. S. Yang, S. Ryu, S. I. Seok, Solvent Engineering for High-performance Inorganic-organic Hybrid Perovskite Solar Cells, Nat. Mater., Vol. 13, 2014, pp. 897-903, https://doi.org/10.1038/nmat4014.
[18] M. Wang, K. Ishii, Photochemical Properties of Phthalocyanines with Transition Metal Ions, Coord Chem Rev., Vol. 468, 2022, pp. 214626, https://doi.org/10.1016/j.ccr.2022.214626.
[19] J. Mack, M. J. Stillman, N. Kobayashi, Application of MCD Spectroscopy to Porphyrinoids, Coord Chem Rev., Vol. 251, 2007, pp. 429-453, https://doi.org/10.1016/j.ccr.2006.05.011.
[20] J. Tauc, A. Menth, States in the Gap, J. Non. Cryst. Solids, Vol. 8-10, 1972, pp. 569-585, https://doi.org/10.1016/0022-3093(72)90194-9.
[21] J. Mack, M. J. Stillman, Assignment of the Optical Spectra of Metal Phthalocyanines Through Spectral Band Deconvolution Analysis and ZINDO Calculations, Coord Chem Rev., Vol. 219-221, 2001, pp. 993-1032, https://doi.org/10.1016/S0010-8545(01)00394-0.
[22] W. Xu, Y. Guo, X. Zhang, L. Zheng, T. Zhu, D. Zhao, W. Hu, X. Gong, Room-Temperature-Operated Ultrasensitive Broadband Photodetectors by Perovskite Incorporated with Conjugated Polymer and Single-Wall Carbon Nanotubes, Adv. Funct. Mater., Vol. 28, 2018, pp. 1705541. https://doi.org/10.1002/adfm.201705541.
[23] Q. Wali, M. Aamir, A. Ullah, F. J. Iftikhar, M. E. Khan, J. Akhtar, S. Yang, Fundamentals of Hysteresis in Perovskite Solar Cells: From Structure-Property Relationship to Neoteric Breakthroughs, Chem. Rec., Vol. 22, 2022, pp. e202100150, https://doi.org/10.1002/tcr.202100150.